Journal of Electroceramics, 14, 293–301, 2005

Impedance/Dielectric Spectroscopy of Electroceramics—Part 2: *Grain Shape Effects and Local Properties of Polycrystalline Ceramics*

N.J. KIDNER,[1] Z.J. HOMRIGHAUS,[1] B.J. INGRAM,[1] T.O. MASON[1] & E.J. GARBOCZI[2]

[1]*Department of Materials Science and Engineering and Materials Research Center, Northwestern University, Evanston, IL 60208, USA*
[2]*Materials and Construction Research, Building and Fire Research Laboratory, National Institute of Standards and Technology, Gaithersburg, MD 20899, USA*

Submitted July 20, 2004; Revised December 29, 2004; Accepted January 4, 2005

Abstract. The reduction of grain size from the microcrystalline regime into the nanocrystalline regime is known to produce significant changes in the transport properties of polycrystalline ceramics. Part 1 of this series [1] described the development of a pixel-based finite-difference "nested-cube model" (NCM), which was used to evaluate existing composite models for the electrical/dielectric properties of polycrystalline ceramics over the entire range of grain core vs. grain boundary volume fractions, from the nanocrystalline regime to the microcrystalline regime. Part 2 addresses grain shape and periodicity effects in such composite modeling, and the extraction of local materials properties (conductivity, dielectric constant) from experimental impedance/dielectric spectroscopy data.

Keywords: impedance, dielectric, effective medium, brick layer model, nested cube model

Introduction

Impedance Spectroscopy (IS) is a powerful, non-destructive technique that has been widely used to characterize the electrical properties of conventional microcrystalline electroceramics [2]. In order to correlate the impedance/dielectric spectroscopy (I/DS) data with the different electro-active regions in the microstructure (grain core, grain boundary) a suitable electrical analogy is required. In Part 1 of this paper [1], the applicability of existing boundary-layer and effective-media models to describe the electrical behavior of nanocrystalline eletroceramics was investigated. Boundary-layer models, widely used to model microcrystalline electroceramics [3], were found to be appropriate at high grain core volume fractions (thin grain boundaries), but they were found to poorly describe the electrical behavior when the grain core volume fraction (ϕ) was reduced (e.g., in the nanocrystalline regime). This is because boundary-layer models are unable to describe the complex current distribution within the nanoscale microstructure. For example, the series BLM (S-BLM) ignores side-wall grain boundary contributions, i.e., the "parallel path" in Fig. 1(a). The series/parallel BLM (SP-BLM) [4] accounts for side-wall contributions by connecting the side-wall grain boundary path in parallel with the serial grain core/grain boundary path, (see Fig. 1(a)), but these paths are separate, with no interchange of current between paths. This limitation was overcome by development of a pixel-based finite-difference model to calculate the electrical properties, and actual current distributions, for the BLM structure [1]. Termed the "nested-cube model" (NCM), it consists of a 3D array of cubic grain cores arranged on a simple cubic lattice separated by homogeneous grain boundary layers; a unit cell of the NCM is shown in Fig. 1(b). The NCM is not analytically tractable and therefore the electrical properties were solved numerically. A thorough description of the numerical model is given in Part 1 [1].

Another approach to modeling the electrical properties of electroceramics is by means of effective medium theory. For low grain core volume fractions, the models of Maxwell-Wagner (MW) [5,6] and Zuzovsky and Brenner (ZBM) [7] are in very good agreement. The MW model is equivalent to the Hashin-Shtrikman [8] upper and lower bounds for conductivity of an isotropic two-phase mixture. We henceforth refer to this model

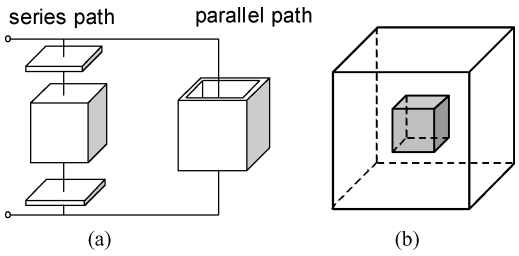

Fig. 1. Schematic representations for (a) the brick-layer model (BLM) and (b) the unit cell of the nested cube model (NCM).

as the MW-HS model. The ZBM consists of a spatially periodic array (e.g., simple cubic) of spherical particles in a continuous isotropic matrix; the simple cubic unit cell is identical to the NCM, (Fig. 1(b)), except with spherical instead of cubic grain cores. The slight difference between these models and the NCM at small grain core volume fractions is expected based on the difference in grain core geometry (spheres vs. cubes). This will be discussed in detail later in this paper. The ZBM is only valid below the percolation threshold (for a simple cubic lattice of monosized spheres, the percolation threshold (ϕ_t) is approximately 0.52). The MW-HS model does not have a percolation threshold and is valid over the entire volume fraction range.

Figure 2 summarizes the findings of Part 1 [1] for the various boundary-layer and effective medium models considered. The DC electrical conductivity for each model is normalized by the DC conductivity of the MW-HS model. In each case, the ratio of grain core-to-grain boundary conductivity was set at $(\sigma_{gc}/\sigma_{gb}) = 1000$. Because the grain boundaries are less conductive than the grain cores, the MW-HS model (the horizontal line at $\sigma/\sigma_{MW\text{-}HS} = 1.0$) represents the lower bound of conductivity for an isotropic two-phase composite. Any predictions below the MW-HS horizontal line, e.g., the brick-layer models (S-BLM and SP-BLM), are physically unrealistic. The brick-layer models are appropriate electrical descriptions only at grain core volume fractions approaching unity (thin grain boundaries) and are not suitable for describing nanoceramic behavior.

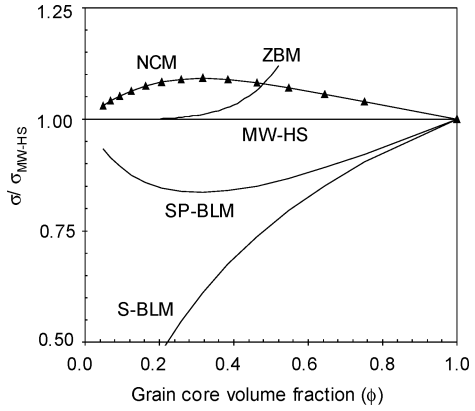

Fig. 2. Normalized DC conductivity (conductivity divided by the conductivity given by the MW-HS model) vs. grain core volume fraction for various microstructural models. The ratio of grain core-to-grain boundary conductivity was set at $(\sigma_{gc}/\sigma_{gb}) = 1000$.

As mentioned above, the ZBM and MS-HS models are in close agreement at grain core volume fractions less than 0.25. This is to be expected, given the spherical grain cores involved in both cases. The rapid conductivity increase of the ZBM beyond $\phi = 0.25$ corresponds to the mutual approach of the spherical grain cores towards the onset of percolation at $\phi = 0.52$. The ZBM is not valid beyond the percolation threshold.

The only model other than the MW-HS to span the entire range of grain core volume fractions is the nested-cube model. The agreement between the NCM and the MW-HS at all volume fractions is noteworthy. A similar agreement between the MW-HS model and a lattice of isotropic cubes was reported by Whites and Wu [9]. They argued that the minimal polarization in a lattice of cubes, due to mutual interactions between the edges and corners of adjacent cubes, leads to a reduction in the effective permittivity to a level very close to the MW-HS lower bound.

Although both NCM and MW-HS models span the entire range of grain core volume fractions, there are two remaining issues to be addressed in the present work. First, neither model is an exact representation of an equiaxed polycrystalline ceramic. The NCM, as represented by the unit cell in Fig. 1(b), consists of cubic grain cores in a periodic arrangement, whereas actual microstructures are more complicated (e.g., dodecahedral grains, non-periodically arranged). Even with cubic-shape grains, Lubomirsky et al. demonstrated significant overlap of space charge regions at grain boundaries and grain corners [10]. On the other hand, the MW-HS model, as shown in Fig. 3, is a non-periodic, space-filling array of self-similar coated grain cores of widely varying sizes. Second, the NCM is mathematically intractable, and can only be solved numerically. This makes it difficult to extract local property values from existing impedance/dielectric

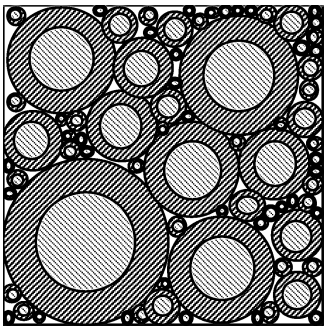

Fig. 3. Schematic representation of the MW-HS model.

spectroscopy (I/DS) data. The present work addresses grain shape (and periodicity) effects in electrocomposite modeling, and the extraction of local electrical/dielectric properties from experimental data.

Details of the Numerical Model

Specifics of the numerical model used to solve the NCM are given in Part 1 [1]. A FORTRAN-77 finite difference numerical program, named ac3d.f, was modified to perform pixel-based computer calculations at finite frequencies. A given "microstructure" is represented as a 3D digital image. Each pixel of the image is treated as a homogeneous phase of known admittance, the admittance being modelled by a parallel (RC) circuit. For the NCM, pixels are assigned to either the grain core or the grain boundary. A diagonalized complex conductivity is assigned to the two phases. A system size ranging from 20^3 to 80^3 pixels is employed to represent the 3D structure of the NCM. In the computation process, each pixel has six orthogonal (RC) circuits extending from its center to the boundaries of the pixel. Neighboring pixels are connected by joining the two bonds together producing a 3D electrical network with a finite difference node at the center of each pixel. A conjugate gradient method is used to solve Laplace's equation at each frequency to give the complex conductivity of the microstructure. Real and imaginary conductivities are then converted to impedance quantities using standard equations.

To generate the periodic simple cubic lattice of the NCM, it was necessary to add a shell of imaginary states around the central grain and grain boundaries to maintain periodic boundary conditions. For a given grain core volume fraction, the system size was varied to assess the effect of spatial resolution. A plot of conductivity versus $1/N$ (where N is the number of pixels) was extrapolated to give the conductivity at $1/N \to 0$. The computational uncertainty associated with the NCM, due to the use of the $1/N$ extrapolation is very small, less than one percent.

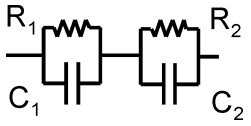

Fig. 4. Standard equivalent circuit.

Analytical equations exist for the resistance/conductance of the other models considered, which could therefore be evaluated in terms of complex conductivities. The same standard equations were employed in each case to convert to impedance format.

Once impedance (Z-plane) plots were generated, commercial software ("Equivalent Circuit" [11]) was used to fit the spectra in terms of the standard equivalent circuit shown in Fig. 4. The resulting R and C values were then used to extract local property values (conductivity and dielectric constant) as a test of the extraction procedure to be described later.

Results and Discussion

A comparison of the various models, both brick-layer and effective medium, is shown in Fig. 2 for the case of resistive grain boundaries ($\sigma_{gc}/\sigma_{gb} = 1000$). In each case, conductivity was normalized by that of the MW-HS model. As mentioned previously, the brick-layer model values fall below those of the MW-HS lower bound (the horizontal line at $\sigma/\sigma_{\text{MW-HS}} = 1.0$), such that they are physically unrealistic. The ZBM is in good agreement with the MW-HS model at low grain core volume fractions (ϕ), but deviates strongly as its percolation threshold is approached ($\phi = 0.52$). The NCM behavior deviates slightly from the MW-HS model, but approaches it at both extremes. In fact, with the exception of the ZBM, due to its percolation threshold, all the models approach the MW-HS behavior at high grain core volume fractions (thin grain boundaries).

McLachlan et al. [12] showed that the impedance/dielectric responses of the brick-layer models and the MW-HS model become indistinguishable at high grain core volume fractions. It would appear that thin coat-

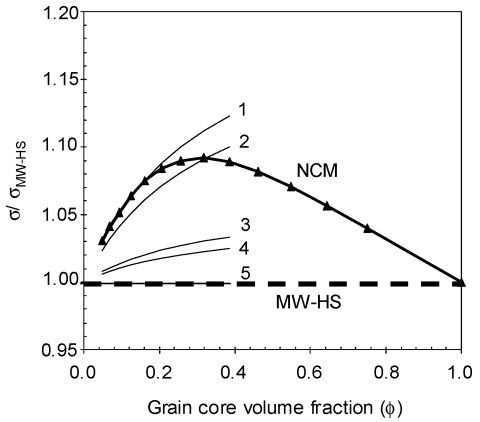

Fig. 5. Differences between the NCM and MW-HS vs. grain core volume fraction for $(\sigma_{gc}/\sigma_{gb}) = 1000$. Superimposed are "dilute limit" conductivities vs. grain core volume fraction plots for two phase composites involving isolated high conductivity particles of various shapes in a less conductive matrix. (1) Cube, (2) Octahedron, (3) Dodecahedron, (4) Icosahedron, (5) Sphere.

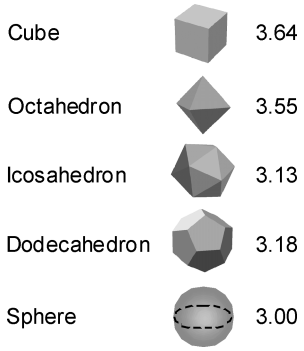

Fig. 6. Intrinsic conductivities for the various shapes studied.

ings behave identically, regardless of grain morphology (i.e., spheres vs. cubes). Similarly, finite element analyses on "real" 2D microstructures [13–15] found close agreement with "cubic" brick-layer structure results, as long as the grains remained monosized and equiaxed. This means that simplified morphologies, whether spherical (e.g., in the MW-HS model) or cubic (e.g., in the brick-layer models, including the NCM) can adequately describe the impedance/dielectric response of "real" electroceramics in the high grain core volume fraction regime (i.e., microcrystalline ceramics with thin grain boundary layers). Furthermore, periodicity appears to be unimportant, since periodic (brick-layer models) and non-periodic microstuctures (e.g., MW-HS) yield similar results.

In the opposing limit (i.e., small grain cores), grain core shape plays a more significant role. Figure 5 shows the difference between the NCM and the MW-HS model for the case where $\sigma_{gc}/\sigma_{gb} = 1000$. Superimposed on the plot are "dilute limit" conductivities vs. volume fraction plots for two-phase composites involving isolated high conductivity particles of various shapes in a less conductive matrix. Each shape of particle has an "intrinsic conductivity" ($[\sigma]_\Delta$), the first order coefficient of dispersed phase volume fraction (ϕ) in the following equation [16]:

$$\frac{\sigma}{\sigma_m} = 1 + [\sigma]_\Delta \phi + 0(\phi^2) + \cdots \qquad (1)$$

where σ is the conductivity of the composite, σ_m is the conductivity of the matrix phase, Δ is σ_p/σ_m where σ_p is the conductivity of the dispersed particles, and higher order terms are neglected. Figure 6 shows the various shapes under consideration, along with their reported intrinsic conductivities (for $\Delta = \infty$) [17]. (A value of $\sigma_p/\sigma_m = 1000$ is essentially the same as $\Delta = \infty$.) The deviation in Fig. 5 of the NCM from the MW-HS model at small grain core volume fractions is clearly due to the different shape of particles. Highly conductive cubes have an intrinsic conductivity of 3.64 whereas spheres have an intrinsic conductivity of 3.0. The dilute limit behavior for isolated cubes matches the NCM results at small grain core volume fractions. Similarly, the dilute limit behavior for isolated spheres precisely matches the MW-HS results (both are horizontal lines at $\sigma/\sigma_{MW-HS} = 1.0$). In between the NCM and the MW-HS model, in decreasing order are octahedral particles ($[\sigma]_\Delta = 3.55$), dodecahedral particles ($[\sigma]_\Delta = 3.18$), and icosahedral particles ($[\sigma]_\Delta$), $= 3.13$). The deviation from the MW-HS model decreases as the shape of particle more closely approximates that of a sphere (e.g., icosahedra and dodecahedra). It should be stressed that these two polyhedral shapes—isosahedra and dodecahedra—are most often employed to model grain shape in polycrystalline materials.

Although neither the NCM nor the MW-HS are realistic microstructural representations of actual polycrystalline ceramics, they represent probable upper and lower bounds for their impedance/dielectric response. In fact, the MW-HS is the absolute lower bound for isotropic two-phase composites with a less conductive matrix (grain boundary) phase. In what follows we consider the calculated difference between the NCM and the MW-HS model as an estimated upper limit for the

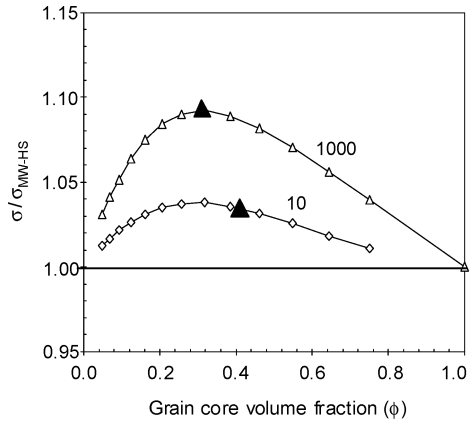

Fig. 7. Differences between the MW-HS and NCM for different ratios of grain core-to-grain boundary conductivities, 10 and 1000.

difference between true polycrystalline ceramic behavior and that of the MW-HS model.

The difference between the NCM and the MW-HS model is dependent upon the ratio of conductivities (σ_{gc}/σ_{gb}), as shown in Fig. 7. At a grain core-to-grain boundary conductivity ratio of 10, the maximum difference between the two models is approximately 3%, increasing to a maximum of approximately 9% at a ratio of 1000. There is little or no change beyond this point, i.e., at still higher grain core-to-grain boundary conductivity ratios. In every case, the maximum difference occurs at a grain core volume fraction of approximately 0.30. The triangular point on each curve will be referred later.

We now turn to the extraction of local electrical properties (conductivity, dielectric constant) from experimental impedance/dielectric spectra. This was first accomplished using the S-BLM [18], which is appropriate only in the case of relatively thin grain boundaries. In a theoretical analysis of nanocrystalline ceramics using the SP-BLM, Bouchet and co-workers [19] found that experimental determination of the electrical properties of nanocrystalline ceramics by impedance spectroscopy is complicated by the superposition of parallel and serial paths (see Fig. 1(a)). Numerical fitting was required to resolve the different materials properties. Bonanos and Lilley [20] derived an equivalent circuit analogy for the MW-HS model by rationalizing and comparing terms of equal power of angular frequency (ω). The equivalent circuit consists of two parallel RC networks connected in series, as shown in Fig. 4. This equivalent circuit is identical to the circuit for the S-BLM however, unlike the S-BLM, the circuit parameters contain terms relating to the material parameters of *both* phases. Therefore each RC element is a combination of the two phases.

$$R_1 = \frac{1}{\sigma_{gb}}\left(\frac{\sigma_{gb}B_\varepsilon - \varepsilon_{gb}B_\sigma}{\sigma_{gb}A_\varepsilon - \varepsilon_{gb}A_\sigma}\right) \tag{2}$$

$$R_2 = \frac{1}{A_\sigma}\left(\frac{A_\varepsilon B_\sigma - A_\sigma B_\varepsilon}{\sigma_{gb}A_\varepsilon - \varepsilon_{gb}A_\sigma}\right) \tag{3}$$

$$C_1 = \varepsilon_{gb}\left(\frac{\sigma_{gb}B_\varepsilon - \varepsilon_{gb}B_\sigma}{\sigma_{gb}A_\varepsilon - \varepsilon_{gb}A_\sigma}\right)^{-1} \tag{4}$$

$$C_2 = A_\varepsilon\left(\frac{A_\varepsilon B_\sigma - A_\sigma B_\varepsilon}{\sigma_{gb}A_\varepsilon - \varepsilon_{gb}A_\sigma}\right)^{-1} \tag{5}$$

where R_1 and C_1 correspond to the grain boundary/low frequency arc (or rightmost arc in Z-plane plots) and R_2 and C_2 correspond to the grain core/high frequency arc (or leftmost arc in Z-plane plots). The coefficients were determined to be:

$$A_\sigma = 2\sigma_{gb} + \sigma_{gc} - 2\phi(\sigma_{gb} - \sigma_{gc}) \tag{6}$$

$$B_\sigma = 2\sigma_{gb} + \sigma_{gc} + \phi(\sigma_{gb} - \sigma_{gc}) \tag{7}$$

$$A_\varepsilon = 2\varepsilon_{gb} + \varepsilon_{gc} - 2\phi(\varepsilon_{gb} - \varepsilon_{gc}) \tag{8}$$

$$B_\varepsilon = 2\varepsilon_{gb} + \varepsilon_{gc} + \phi(\varepsilon_{gb} - \varepsilon_{gc}). \tag{9}$$

By manipulation of Eqs. (2)–(9), we were able to derive four equations for the materials parameters in terms of the circuit parameters (R_1, C_1, R_2, C_2) in Fig. 4, which can be determined from complex impedance plots if one knows the grain core volume fraction (ϕ). The four equations are:

$$\sigma_{gb} = \frac{(1-\phi)}{R_1(1+2\phi)} \tag{10}$$

$$\sigma_{gc} = \frac{-2R_2(\phi-1)^2 + R_1 9\phi}{R_1R_2(1+2\phi)^2} \tag{11}$$

$$\varepsilon_{gb} = \frac{C_1(1-\phi)}{1+2\phi} \tag{12}$$

$$\varepsilon_{gc} = \frac{-2C_1(1-\phi)^2 + 9C_2\phi}{(1+2\phi)^2}. \tag{13}$$

Given the grain core volume it is possible to calculate the local electrical properties (conductivity, dielectric constant) of both grains and grain boundaries. Unfortunately, it is virtually impossible to establish the

volume fractions of grains cores/boundaries by independent means (e.g., electron microscopy), especially given the fact that electrical width (e.g., due to space charge layers) and structural width (e.g., due to a discrete phase) can be quite different.

Using Eqs. (10)–(13), however, we can come up with a good estimate for the grain core volume fraction and effective grain boundary (electrical) width. This is done by fitting an experimental Z-plane plot with dual arcs using commercially available software (e.g., "Equivalent Circuit" [11]) for the terms R_1, C_1, R_2, and C_2. Then Eq. (13) is plotted as ε_{gc} vs. grain core volume fraction. By constraining the value of ε_{gc} thus obtained to be consistent with published bulk values for the material in question, we arrive at an estimate for the grain core volume fraction, and can proceed to calculate the other parameters in Eqs. (10)–(13).

We made two simulations, using the NCM, of impedance response at or near the volume fractions corresponding to the maximum difference between the NCM and the MW-HS model in Fig. 7. The first was made at a grain core volume fraction of $\phi = 0.42$. The ratios of grain-core-to-grain-boundary properties were set at $(\sigma_{gc}/\sigma_{gb}) = 10$ and $(\varepsilon_{gc}/\varepsilon_{gb}) = 0.1$, based upon grain core values of 10 and 3×10^{-4} S/cm for dielectric constant and conductivity, respectively. This corresponds to the triangular point on the lower curve in Fig. 7. The resulting NCM Z-plane plot is shown in Fig. 8(a). The non-linear least-squares fitting routine of the deconvolution software [11] was used to find the circuit parameters (R_1, C_1, R_2, C_2). These parameters were then inserted into Eqs. (10)–(13). Figure 8(b) shows dielectric constant vs. grain core volume fraction and Fig. 8(c) shows conductivity vs. grain core volume

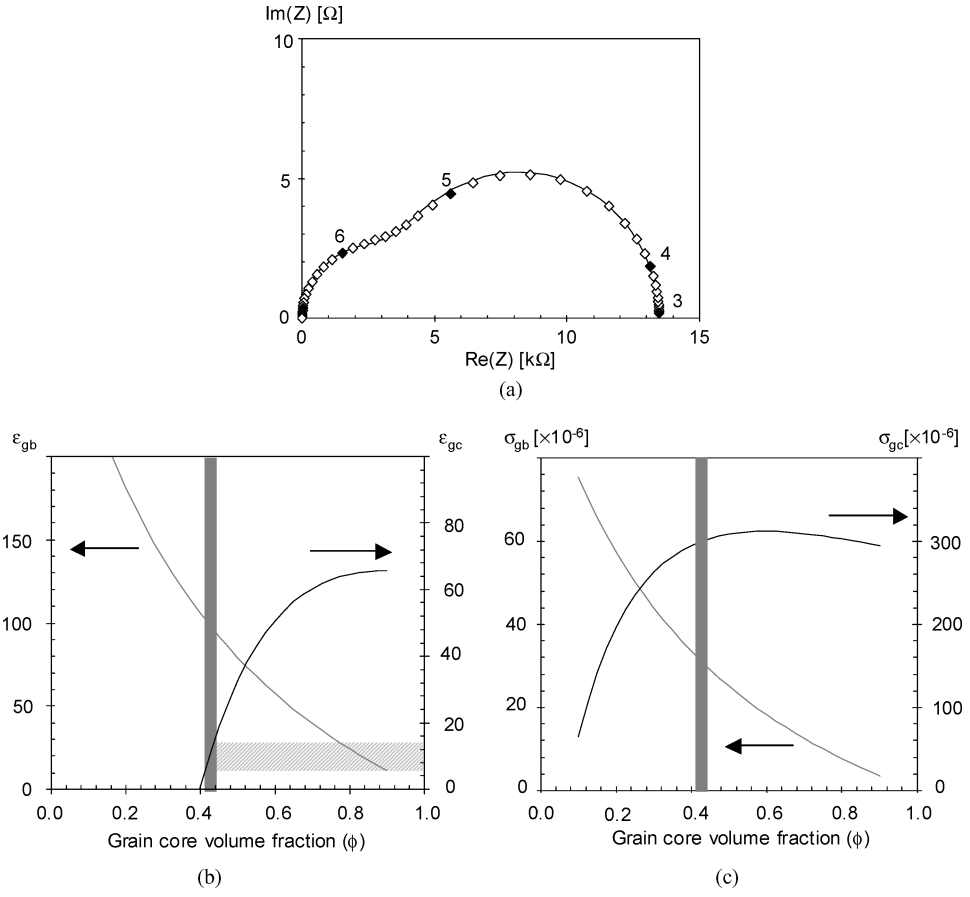

Fig. 8. (a) Simulated impedance response for NCM assuming $\sigma_{gc}/\sigma_{gb} = 10$ and $\varepsilon_{gc}/\varepsilon_{gb} = 0.1$ and a grain core volume fraction of 0.42, with log(frequency) markers as shown. The solid line shows the non-linear least squares fit. (b) shows dielectric constant vs. grain core volume fraction, and (c) conductivity vs. grain core volume fraction for both grain core and grain boundary phases using Eqs. (11)–(14).

Table 1. Fitted materials parameters for the circuit parameters determined from Fig. 8(a).

Material property	Input value	Range for ($\varepsilon_{gc} \pm 50\%$)
Grain boundary dielectric (ε_{gb})	100	94–103
Grain boundary conductivity (σ_{gb})	3×10^{-5}	$(3.00–3.26) \times 10^{-5}$
Grain core conductivity (σ_{gc})	3×10^{-4}	$(2.97–3.02) \times 10^{-4}$

fraction for both grain core and grain boundary phases. By constraining ε_{gc} to be within 50% of the known value ($\varepsilon_{gc} = 10 \pm 5$), the allowed grain core volume fraction must be between 0.40 and 0.44. Table 1 gives the corresponding ranges of the three unknown material properties based on this uncertainty in grain core volume fraction.

In spite of relatively large bounds on the known parameter (ε_{gc}), the bounds on the other parameters are relatively narrow, and the agreement with the NCM input parameters is quite good.

The other simulation was at a grain core volume fraction of 0.32, corresponding to the triangular point in the upper curve of Fig. 6. In this case the ratios of grain-core-to-grain-boundary properties were set at (σ_{gc}/σ_{gb}) = 1000 and ($\varepsilon_{gc}/\varepsilon_{gb}$) = 0.1, based upon grain core values of 3×10^{-4} S/cm and 10 for conductivity and dielectric constant, respectively. The resulting NCM Z-plane plot is shown in Figs. 9(a) and (b). The non-linear least-squares fitting routine of the deconvolution software [11] was used to find the circuit

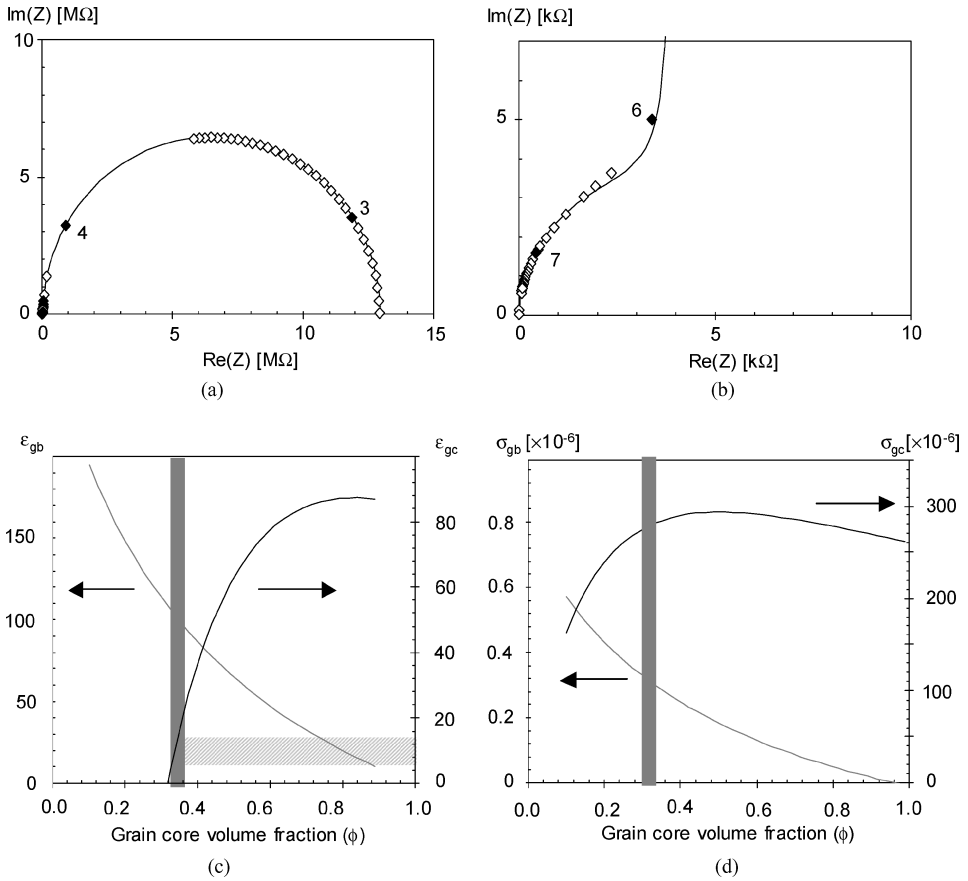

Fig. 9. (a) Simulated impedance response for NCM assuming $\sigma_{gc}/\sigma_{gb} = 1000$ and $\varepsilon_{gc}/\varepsilon_{gb} = 0.1$ and a grain core volume fraction of 0.32, with log(frequency) markers as shown. The solid line shows the non-linear least squares fit. (b) enlarges the high frequency region to show the grain core arc. (c) shows the dielectric constant vs. grain core volume fraction, and (d) conductivity vs. grain core volume fraction for both grain core and grain boundary phases using Eqs. (11)–(14).

Table 2. Fitted materials parameters for the circuit parameters determined from Fig. 9(a).

Material property	Input parameters	Range for ($\varepsilon_{gc} \pm 50\%$)
Grain boundary dielectric (ε_{gb})	100	99–106
Grain boundary conductivity (σ_{gb})	3×10^{-7}	$(2.96–3.17) \times 10^{-7}$
Grain core conductivity (σ_{gc})	3×10^{-4}	$(2.80–2.84) \times 10^{-4}$

parameters (R_1,C_1,R_2,C_2). These parameters were then inserted into Eqs. (10)–(13). Figure 9(b) shows dielectric constant vs. grain core volume fraction and Fig. 9(c) shows conductivity vs. grain core volume fraction for both grain core and grain boundary phases. By constraining ε_{gc} to be within 50% of the known value ($\varepsilon_{gc} = 10 \pm 5$), the allowed grain core volume fraction must be between 0.325 and 0.350. Table 2 gives the corresponding ranges of the three unknown material properties based on this uncertainty in grain core volume fraction.

Again, in spite of relatively large bounds on the known parameter (ε_{gc}), the bounds on the other parameters are relatively narrow. Whereas the agreement with NCM grain boundary input parameters is acceptable, the grain core conductivity is too small by ~6–7% which is not unexpected given the ~9% difference in overall conductivity between the two models in Fig. 7.

It should be stressed that we are employing a MW-HS model-based analysis procedure to extract local grain core/boundary properties from a nested-cube microstructure and associated impedance plots. Our success in doing so bodes well for analysis of impedance spectra for actual polycrystalline microstructures. Based upon the data in Fig. 5, the difference between the impedance response of actual microstructures (e.g., dodecahedral grain cores) and the MW-HS model should be smaller than for the NCM.

This said, we have not exhaustively considered all possible combinations of the five variables (σ_{gc}, ε_{gc}, σ_{gb}, $\varepsilon_{gb,}\phi$), especially combinations involving conductive grain boundaries and resistive grain cores ($\sigma_{gb} > \sigma_{gc}$). Nevertheless, the extraction procedure of Eqs. (10)–(13) appears to be robust and reliable for all combinations considered to date involving $\sigma_{gc} > \sigma_{gb}$ (resistive grain boundaries).

In the case of very thin grain boundaries ($\phi \rightarrow 1$), however, it is impossible to obtain the grain boundary volume fraction (1-ϕ) and thereby the grain boundary thickness with any confidence.

There are several caveats, in applying Eqs. (10)–(13) to the extraction of local electrical/dielectric properties from impedance data on actual specimens. First of all, the microstructures involved must be monosized and equiaxed. Second, the time constants (RC products) of the grain core and grain boundary arcs must be sufficiently different to resolve two arcs in the impedance spectra. This requires at least an order of magnitude RC difference between them [21]. Third, neither arc should be significantly depressed below the "real" axis in Z-plane plots. In prior work we considered the issue of arc depression, and showed that if both arcs were comparably (and only slightly) depressed, an analysis for local properties could still be made [21]. If one arc is significantly more depressed than the other, however, reliable deconvolution becomes quite difficult. Finally, the approach does not allow for spatially varying properties, e.g., conductivity varying with distance from the physical grain boundary (e.g., due to space charge layers). For very small grain core volume fractions the grain cores are unlikely to be homogeneous, the transition region between the grain core and grain boundary will become important, leading to spatially varying properties. Future work will address such complications.

Conclusions

Of several models considered, only the nested-cube model (NCM) and the Maxwell-Wagner/Hashin-Shtrikman (MW-HS) model are capable of describing the electrical/dielectric properties of polycrystalline ceramics over the entire range of grain core volume fractions, from high (microcrystalline) to low (nanocrystalline). The other models fail due to unrealistic current distributions (the series and series/parallel brick-layer models, S-BLM, SP-BLM) or exhibit a percolation threshold (the Zuzovsky-Brenner Model, ZBM).

The nested cube model (NCM) was used to investigate the influence of grain shape and periodicity on the electrical/dielectric properties of polycrystalline ceramics. At high grain core volume fractions (thin grain boundaries), consistent with micro-structured ceramics, boundary-layer models (S-BLM, SP-BLM, NCM) and effective medium models (MS-HS model) do equally well in describing behavior. Neither grain shape nor periodicity seem to matter. (The brick-layer

models are periodic, whereas effective media models are not.) At low grain core volume fractions (thick grain boundaries), consistent with nano-structured ceramics, grain shape plays a more important role. The differences between models (NCM, MW-HS) are small, but noticeable, and reflect the different "intrinsic conductivities" of the grain core "particles" involved (e.g., 3.64 for cubes vs. 3.0 for spheres). The close match between the ZBM and the MW-HS model at small grain core volume fractions is to be expected, based upon the spherical particles in each case. Smaller differences (than with the NCM) are anticipated between "real" polycrystalline ceramics, with icosahedral or dodecahedral grains (and intrinsic conductivities of 3.13 and 3.18, respectively), and MW-HS effective medium theory.

Microstructurally, the NCM can be considered as the "worst case" difference with the MW-HS model. It was employed to generate "experimental" impedance data, from which equivalent circuit (RC)(RC) elements were obtained by linear least-squares fitting. These parameters were employed to calculate grain core volume fraction and local electrical/dielectric properties (grain core and grain boundary), based upon a set of equations derived from the Lilley-Bonanos [20] treatment of the MW-HS equation. The procedure involves constraining the grain core dielectric constant to be within a specified range of published bulk values. Even with relatively large bounds, the bounds on the grain core volume fraction are small, enabling the other parameters to be determined. The agreement with actual input parameters is quite good, within a few percent in the worst possible case.

It must be stressed that neither the NCM nor the MW-HS model are accurate representations of "real" electroceramic microstructures. Nevertheless, based upon grain shape and intrinsic conductivity arguments, the anticipated differences between the electrical/dielectric behavior of such microstructures, if monosized and equiaxed, and that of the MW-HS should be smaller than for the NCM. This suggests that the procedure we have demonstrated for extracting local properties from a nested-cube microstructure should be even more reliable for extracting local properties from "real" microstructures.

Acknowledgments

This work was supported in part by the U.S. Department of Energy under grant no. DE-FG02-84ER45097 and in part by the National Science Foundation under grant no. DMR-0076097 through the Materials Research Science and Engineering Center program.

References

1. N.J. Kidner, Z.J. Homrighaus, B.J. Ingram, T.O. Mason, and E.J. Garboczi., *J. Electroceram.*, **14**, 283–291 (2005).
2. J.T. Irvine, D.C. Sinclair, and A.R. West, *Adv. Mater*., **2**(3), 132 (1990).
3. N.M. Beekmans and L. Heyne, *Electrochim. Acta*, **21**, 303 (1976).
4. H. Näfe, *Solid State Ionics*, **13**, 255 (1984).
5. J.C. Maxwell, *A Treatise on Electricity and Magnetism* (Clarendon Press, Oxford, 1881).
6. K.M. Wagner, in *Arkiv Electrotechnik*, edited by H. Schering (Springer-Verlag, Berlin, 1914).
7. M. Zuzovsky and H. Brenner, *J. Appl. Math. Phys*., **28**(6), 979 (1977).
8. Z. Hashin and S. Shtrikman, *J. Appl. Phys*., **33**, 3125 (1962).
9. F. Wu and K.W. Whites, *IEEE Trans. Microwave Theory Tech*., **50**(7), 1723 (2002).
10. I. Lubomirsky, J. Fleig, and J. Maier, *J. Appl. Phys.*, **92**(11), 6819 (2002).
11. B.A. Boukamp, "Equivalent Circuit (EQUIVCRT.PAS)", University of Twente, The Netherlands (1990).
12. D.S. McLachlan, J.-H. Hwang, and T.O. Mason, *J. Electoceram*., **5**(1), 37 (2002).
13. J. Fleig and J. Maier, *J. Electrochem. Soc*., **145**, 2081 (1998).
14. J. Fleig and J. Maier, *J. Eur. Ceram. Soc.*, **19**, 693 (1999).
15. R. Hagenbeck and R. Waser, *Ber. Busenges. Phys. Chem.*, **101**, 1238 (1997).
16. E.J. Garboczi and J.F. Douglas, *Phys. Rev. E*, **53**(6), 6169 (1996).
17. M.L. Mansfield, J.F. Douglas, and E.J. Garboczi, *Phys. Rev. E*, **64**(6), 61401 (2001).
18. J.E. Bauerle, *J. Phys. Chem. Solids*, **30**, 2657 (1969).
19. R. Bouchet, P. Knauth, and J.-M. Laugier, *J. Electrochemical Society*, **150**(7), E348 (2003).
20. N. Bonanos and E. Lilley, *J. Phys. Chem. Solids*, **42**(10), 943 (1981).
21. T.O. Mason, J.-H. Hwang, N. Mansourian-Hadvi, G.B. Gonzalez, B.J. Ingram, and Z.J. Homrighaus, in *Nanocrystalline Materials: Synthesis and Characterization*, edited by P. Knauth and J. Schoonman (Kluwer US, Paris, 2001).